TU Delft

Delft University of Technology

Document Version
Final published version

Licence
CC BY-NC-ND

Citation (APA)
Wruck, F., Schmitt, J., Till, K., Fenzl, K., Bertolini, M., Tippmann, F., Katranidis, A., Bukau, B., Tans, S. J., & More Authors (2025). Co-translational ribosome pairing enables native assembly of misfolding-prone subunits. *Nature Communications*, *16*(1), Article 7626. https://doi.org/10.1038/s41467-025-61500-y

Important note
To cite this publication, please use the final published version (if applicable).
Please check the document version above.

Copyright
In case the licence states “Dutch Copyright Act (Article 25fa)”, this publication was made available Green Open Access via the TU Delft Institutional Repository pursuant to Dutch Copyright Act (Article 25fa, the Taverne amendment). This provision does not affect copyright ownership.
Unless copyright is transferred by contract or statute, it remains with the copyright holder.

Sharing and reuse
Other than for strictly personal use, it is not permitted to download, forward or distribute the text or part of it, without the consent of the author(s) and/or copyright holder(s), unless the work is under an open content license such as Creative Commons.

Takedown policy
Please contact us and provide details if you believe this document breaches copyrights.
We will remove access to the work immediately and investigate your claim.

This work is downloaded from Delft University of Technology.

nature communications

Article

https://doi.org/10.1038/s41467-025-61500-y

Co-translational ribosome pairing enables native assembly of misfolding-prone subunits

Received: 12 December 2022

Accepted: 20 June 2025

Published online: 15 August 2025

Check for updates

Florian Wruck[1], Jaro Schmitt[2,7], Katharina Till[1,7], Kai Fenzl[2,5,7], Matilde Bertolini[2,6,7], Frank Tippmann[2], Alexandros Katranidis[3], Bernd Bukau[2], Günter Kramer[2] & Sander J. Tans[1,4]

Protein complexes are pivotal to most cellular processes. Emerging evidence indicating dimer assembly by pairs of ribosomes suggests yet unknown folding mechanisms involving two nascent chains. Here, we show that co-translational ribosome pairing allows their nascent chains to 'chaperone each other', thus enabling the formation of coiled-coil homodimers from subunits that misfold individually. We developed an integrated single-molecule fluorescence and force spectroscopy approach to probe the folding and assembly of two nascent chains extending from nearby ribosomes, using the intermediate filament lamin as a model system. Ribosome proximity during early translation stages is found to be critical: when interactions between nascent chains are inhibited or delayed, they become trapped in stable misfolded states that are no longer assembly-competent. Conversely, early interactions allow the two nascent chains to nucleate native-like quaternary structures that grow in size and stability as translation advances. We conjecture that protein folding mechanisms enabled by ribosome cooperation are more broadly relevant to intermediate filaments and other protein classes.

Cells rely on the faithful production of protein complexes. According to textbook models, newly translated polypeptides first undergo a conformational search for the native tertiary structure[1–3], and then a diffusion-driven assembly into larger complexes[4,5]. This paradigm is challenged by mounting evidence of co-translational assembly, either between a fully-formed diffusing subunit and a nascent chain[6–11] (termed "co-post assembly"), or between two nascent chains[12–15] (termed "co-co assembly"). We recently revealed over 800 co-co assembling homodimers, thus showing the general nature of this biogenesis route[16]. However, the biochemical methods and disome selective ribosome profiling (DiSP)[16] employed thus far do not detect the nascent chain structures nor the conformational changes during the folding and assembly process. Single-molecule fluorescence and optical-tweezers methods have made important advances in studying nascent chain folding but remain limited to single ribosome-nascent chain complexes (RNCs)[3,17,18]. As a result, we lack insight into the conformational basis and functional relevance of protein complex assembly enabled by coupled ribosomes.

Here, we study these issues using the human intermediate filament lamin, whose homodimeric coiled-coil structure represents the largest co-co assembly class[16]. Lamins form a scaffold for the nuclear envelope that spatially organizes chromatin[19,20], with mutants being the root cause for diseases including premature ageing and cardiomyopathies[21]. Lamin A and its splice variant lamin C contain three domains[22–24]: the N-terminal

[1]AMOLF, Amsterdam, The Netherlands. [2]Center for Molecular Biology of Heidelberg University (ZMBH) and German Cancer Research Center (DKFZ), DKFZ-ZMBH Alliance, Heidelberg, Germany. [3]Ernst-Ruska Centre for Microscopy and Spectroscopy with Electrons/ER-C-3 Structural Biology, Forschungszentrum Jülich (FZJ), Jülich, Germany. [4]Bionanoscience Department of Delft University of Technology and Kavli Institute of Nanoscience Delft, Delft, The Netherlands. [5]Present address: European Molecular Biology Laboratory, Heidelberg, Germany. [6]Present address: Addition Therapeutics, South San Francisco, California, USA. [7]These authors contributed equally: Jaro Schmitt, Katharina Till, Kai Fenzl, Matilde Bertolini. e-mail: tans@amolf.nl

https://doi.org/10.1038/s41467-025-61500-y

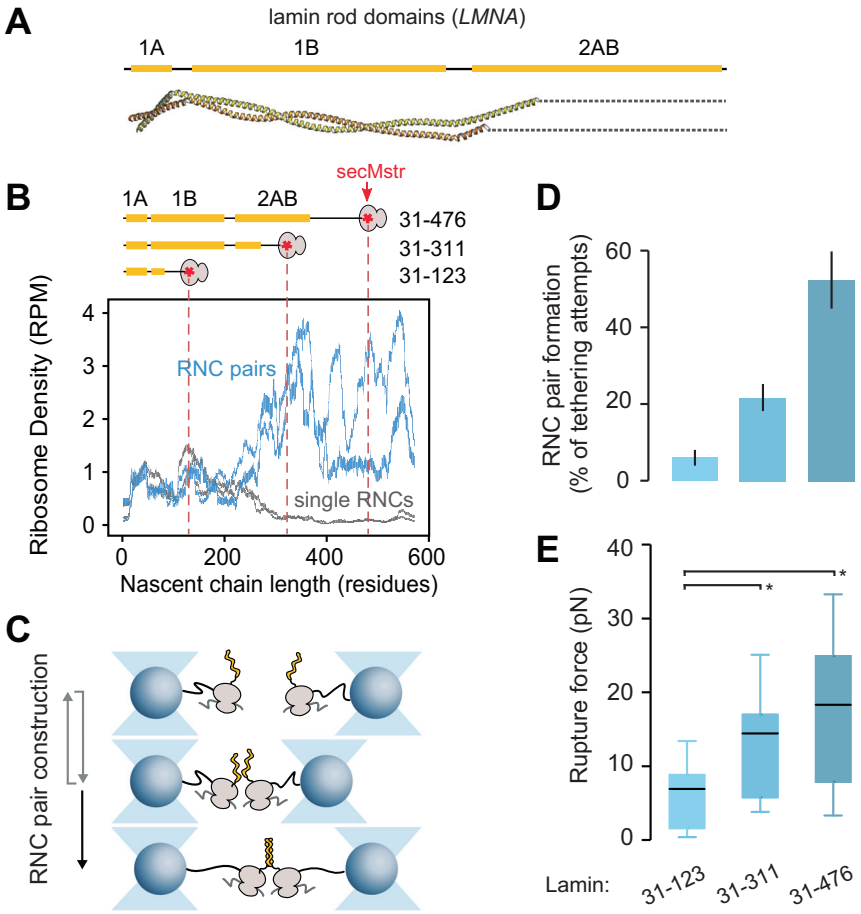

Fig. 1 | Formation of lamin RNC pairs. A Structure of the lamin A/C homodimer showing the coiled-coil rod domains 1A, 1B and a part of domain 2AB (PDB code: 6JLB[67]). **B** Lamin RNC pairing in vivo. Bottom: Ribosome density along the *LMNA* mRNA for RNC pairs (pairing via the nascent chains, blue) and for single RNCs (grey), as obtained by DiSP for U2OS cells, with 150 mM KCl and (Bissulfosuccinimidyl suberate) crosslinker present upon cell lysis. Two replicate data sets are shown, as bars representing the position-wise 95% Poisson confidence intervals corrected for library size and smoothed with 15-codon wide sliding window[16]. RPM: reads per million. Top: Lamin nascent chain fragments for optical tweezer experiments (**C**). Dashed lines: ribosome stalling positions. SecMstr: peptide sequence for efficient translation stalling. Yellow bars: coiled-coil domains. Also indicated are the amino acids of the three fragments. **C** Optical tweezer approach to constitute RNC pairs. Ribosomes, coupled to beads via DNA handles, translate lamin fragments until a secMstr-mediated translation arrest using in vitro transcription-translation. Next, the beads are repeatedly brought together for 5 s, to let nascent chains interact and dimerize, and separated again (grey arrows). A stable tether upon pulling, of twice the DNA handle length, indicates dimer formation (black arrow), while no tether is formed when the chains do not dimerize. RNC cartoon from Bertolini et al.[16]. Reprinted with permission from AAAS. **D** The fraction of dimerization attempts yielding dimer formation, determined as depicted in (**C**), for three lamin fragments ($n = 136$ $LMNA_{31–123}$, $n = 140$ $LMNA_{31–311}$, $n = 46$ $LMNA_{31-476}$ cycles). Error bars are standard error of proportion. **E** Rupture force of nascent chain dimer tethers, as measured by ramping up the tether tension, for three lamin fragments ($n = 8$ $LMNA_{31–123}$, $n = 30$ $LMNA_{31–311}$, $n = 24$ $LMNA_{31–476}$ rupturing events). Boxes indicate 25th and 75th percentiles, whiskers indicate the SD, center line indicates mean. Star: significant difference, $p < 0.05$ (two-sided Mann–Whitney U test, $LMNA_{31-123}$/$LMNA_{31-311}$: $p = 0.036$, $LMNA_{31–123}$/$LMNA_{31–476}$: $p = 0.017$). Source data are provided as a Source Data file.

unstructured head domain, the central α-helical rod domain that mediates dimer formation (Fig. 1A, B, Supplementary Fig. 1), and the C-terminal tail domain with an immunoglobulin-like fold[25]. Lamin polymerization occurs in the nucleus by head-to-tail assembly of lamin homodimers[26]. The lack of lamin heterodimers[27], even though lamin A and C have identical dimerization domains, led to suggestions of a post-translational sorting mechanism that recognizes the different tail domains[28]. Co-co assembly can alternatively promote isoform-specific homomer formation, and more generally avoid promiscuous interactions between conserved oligomerization domains[29].

Results

In vivo detection of lamin nascent chain interactions

We first studied lamin co-co assembly in vivo, including the dependence on cell type (U2OS and HEK cells) and DiSP conditions that can potentially influence the detected assembly onset (Fig. 1B, Supplementary Fig. 2). The DiSP method is based on isolating RNC pairs that are coupled via their nascent chains (disomes), as well as uncoupled RNCs (monosomes), followed by sequencing their protected 30 nucleotide-long RNA footprints as in standard ribosome profiling. Consistent with co-co assembly, the number of mRNA reads for lamin RNC pairs increased after synthesis of coil 1B, as the reads decreased for the uncoupled RNCs[16]. This lamin dimerization transition was robustly observed, and did not depend on factors that can affect nascent chain interactions, such as the salt concentration (150 or 500 mM KCl) or presence or absence of a protein-protein crosslinker (BS3 and EDC, see Supplementary Fig. 2). The robustness of the lamin nascent chain interactions may originate from the comparatively large dimer interface of its coiled-coil structure. Co-translational dimerization is an alternative mechanism to classical post-translational dimer formation, in which monomers find each other by diffusion through the cytosol. However, pull-down experiments on TwinStrep-tagged lamin showed that no wild-type lamin was co-purified[16], further supporting the notion that lamin co-co dimerization occurs in vivo.

In vitro formation of lamin RNC pairs

Approaches to purify RNC pairs from cells, like our DiSP method, are less suited to study nascent chain conformations[16,30,31], due to RNC heterogeneity and the difficulty of incorporating measurement probes. Hence, we aimed to construct RNC pairs in vitro, stalled at key phases of translation identified by the DiSP data: before the onset of dimerization, with only the small α-helical coil 1A fully translated, after the dimerization onset with coils 1A and 1B fully translated, and finally after translation of coil 2AB, with the full-length rod domain translated and ribosome exposed (Fig. 1B).

To construct pairs of RNCs coupled by their nascent chains, we first linked biotinylated ribosomes to polystyrene beads via 5 kb DNA handles (Fig. 1C). Synthesis of lamin nascent chains by the bead-tethered ribosomes was performed by in vitro transcription-translation, using the 'SecM strong'[32] sequence to stall translation at positions indicated above (Fig. 1B, Supplementary Fig. 3). Two such beads were captured by two optical traps, repeatedly brought together, within about 200 nm for about 5 seconds, and separated again. We quantified the fraction of approach-retract cycles in which a tether formed between the beads that was twice the length of a single DNA handle (Supplementary Fig. 4), and hence indicated the coupling of two RNCs via their nascent chains (Fig. 1C). This fraction increased from below 10 % to above 50 % with increasing fragment length (Fig. 1D). Such an increasing trend agrees with the lamin DiSP data (Fig. 1B), and with coupling taking place via the nascent chains, rather than via other (ribosomal) components. While rare, we did detect dimerization events already for the shortest fragment, indicating an earlier assembly onset than detectable by DiSP (Fig. 1B). Interactions between shorter nascent chain dimers may be detected less efficiently by DiSP, while the polysome structure may also reduce their interactions. To probe the stability of the nascent chain dimers against dissociation, we measured the force required to rupture the tether by increasing the distance between the beads. The tethers ruptured in a single step, in line with coiled-coils unfolding and dissociating discretely during pulling[33]. The rupture force indeed increased with fragment length, from about 5 pN to over 15 pN (Fig. 1E), consistent with a progressively larger coiled-coil dimer interface. Based on the DiSP data alone, one cannot formally exclude that lamin nascent chains do not homodimerize, but instead form complexes with other nascent chains. Thus, the in vitro experiments presented here provide direct support for the ability of lamin nascent chain homodimerization. Overall, the data indicated that lamin nascent chains dimerized when brought in close proximity, with associations that start at short chain lengths and become more resistant against forced dissociation with increasing chain length.

We studied how these findings related to coiled-coil structural features, in order to obtain further mechanistic insight (Supplementary Fig. 5). Coiled-coil structures are based on interactions between heptad sequences in each coil, denoted as: $(abcdefg)_n$. Residues at positions a and d are mainly hydrophobic and make up the core of the coiled-coil interface. Coiled-coils have a packing arrangement termed knobs-into-holes (KIH)[34–36], with certain residues like Leucine, Valine, and Isoleucine packing particularly well within this arrangement considering their side chain packing geometries[37,38]. A tabulation of these interactions indicated that going from the short to the intermediate fragment increased the stability the most, while the longest fragment gained less in comparison (Supplementary Fig. 5A–C). The same is concluded when computing the cumulative residue-residue contact energy[39] along the lamin dimer interface (Supplementary Fig. 5D–F). These computations agree with our measurements of the mean rupture force, which doubles from construct 1 to construct 2 (from 7 pN to 14 pN, $p < 0.05$), but increases only marginally to construct 3 (18 pN, $p = 0.5$). Overall, this analysis indicated that most of the lamin dimer stability is contributed by coil 1B, as it has the most heptad repeats and more ideal packing amino acids at the a and d positions, when compared to coils 1A and 2B.

We note that the applied force acts on the inter-chain contacts, as both are perpendicular to the helical axis in our assay (Fig. 1C). Hence, substantial alpha-helical unfolding likely does not occur before inter-strand contacts are broken. This is in line with previous work, which suggests that mechanical unfolding of coiled-coils involves the simultaneous breakage of many intra- and inter-chain contacts[40–43]. We also note that rupture forces between 8 and 15 pN were observed, which is in the same range as the rupture forces observed here (Fig. 1E). In contrast, when the force acts in parallel to the helical axis, helices can elongate before the strands separate[42,44,45].

Nascent lamin complex formation observed by fluorescence

To test whether the observed nascent dimers are consistent with the native coiled-coil lamin structure, we integrated fluorescence detection into the optical tweezers assay (Fig. 2A). We inserted a pair of adjacent cysteines at the lamin N-terminus and reasoned that two such pairs should co-localize in the native parallel coiled-coil conformation. Hence, a bipartite tetra-cysteine motif would form that can bind the

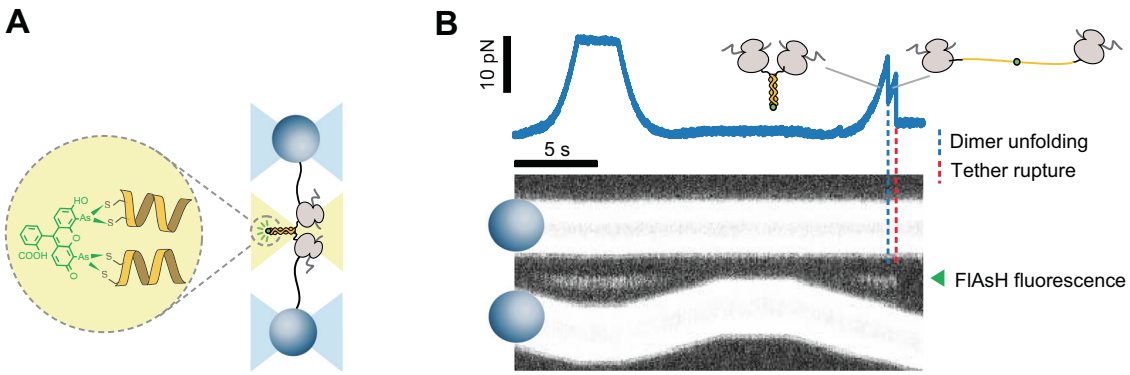

Fig. 2 | Fluorescent detection of nascent lamin dimers. A Approach for visual verification of N-terminal co-localization. Two nascent chains can be linked by the FlAsH dye, which binds to a bipartite tetracysteine motif formed by two cysteines at each N-terminus, if they co-localize as in the native coiled-coil dimer structure (Fig. 1A). Bound FlAsH becomes fluorescent and is detected by scanning a confocal excitation beam (yellow beam, green arrows) along the molecular tether, while the optical tweezers laser beams (blue) trap the beads. **B** Corresponding data. Bottom: detected fluorescence scans in time, showing bead movements in stretch-relax cycles and the FlAsH fluorescence signal between the two beads (green arrowhead). The FlAsH signal is only observed when the tether is under tension and hence stably in focus. RNC pair construct: $LMNA_{31–476}$. Top: corresponding measured force acting on the beads and tether. Blue dashed line: sudden drop in force indicates unfolding, while FlAsH keeps the N-termini connected (**A**). Red dashed line: tether rupture, likely by dissociation of one of the DNA handles from the bead surface. Source data are provided as a Source Data file. RNC cartoon from Bertolini et al.[16]. Reprinted with permission from AAAS.

https://doi.org/10.1038/s41467-025-61500-y

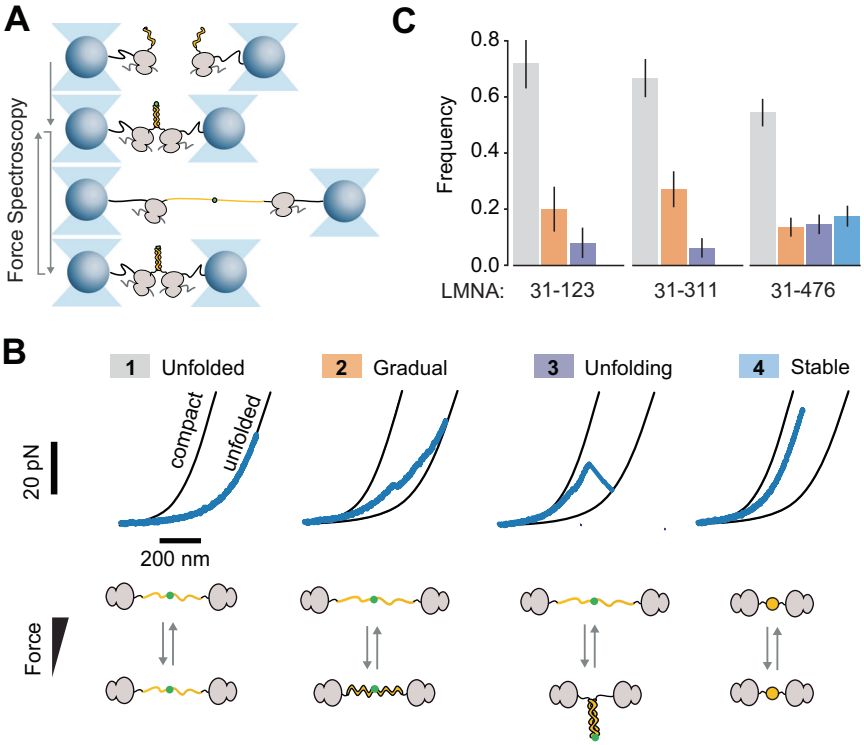

Fig. 3 | Delayed RNC interaction promotes non-native lamin dimer conformations. A Diagram of nascent chain dimer force spectroscopy approach. Lamin nascent chain dimers are formed as depicted in Fig. 1 C, and subsequently exposed to repeated stretching and relaxation while the split-FlAsH-tag (green dot, see also Fig. 2A) keeps N-termini bound together upon unfolding. **B** Classes of force-extension behaviour of lamin nascent chain dimers. Black lines are theoretical worm-like chain (WLC) curves for both nascent chains being compact (left) or fully unfolded (right). The position of the measured data (blue) in between these two reference curves indicates what fraction of the nascent chain (how many amino acids) is in the compact state, and what fraction is in the extended state. During stretch-relax cycles four classes are observed, with the majority of the chain: (1) remaining unfolded, (2) initially compact and extending and compact gradually under tension, as expected for linear α-helices, (3) initially compact and unfolding discretely below 45 pN, as expected for coiled-coil dimer structures, (4) initially compact and remaining so up to 45 pN, typically for multiple stretch-relax cycles, indicative of a kinetically trapped misfolded state. Data are shown for $LMNA_{31–476}$ fragments. **C** Frequency of stretch-relax cycles with observed force-extension features (see panel B), for lamin nascent chain dimers of three nascent chain lengths. $n = 14$ $LMNA_{31–123}$ molecules, 24 pulling cycles, $n = 29$ $LMNA_{31–311}$ molecules, 43 pulling cycles, $n = 54$ $LMNA_{31-476}$ molecules, 100 pulling cycles. Dimer formation and misfolding increases in frequency with increasing nascent chain length, at the expense of unfolded states. $LMNA_{31-311}$ and $LMNA_{31-476}$ are significantly different ($p = 0.002$, Chi^2-test). Error bars: standard error of proportion. Colours are as in panel B. Source data are provided as a Source Data file. RNC cartoon from Bertolini et al.[16]. Reprinted with permission from AAAS.

FlAsH dye[46], which becomes fluorescent upon binding, and detectable by confocal fluorescence imaging. We performed the above approach-retraction protocol to form a lamin RNC pair and exposed it to FlAsH in solution. To detect bound FlAsH, a confocal fluorescence excitation beam was scanned across the beads and along the connecting tether. A fluorescent signal indeed appeared in-between the beads, visible as an additional line in kymographs that display the subsequent fluorescence emission scans (Fig. 2B). Consistent with the formation of an in-register parallel coiled-coil, we detected a FlAsH signal when tethers were formed. As in the measurements without the FlAsH dye (Fig. 1D), the longer fragments again showed higher dimer formation frequency (Supplementary Fig. 6).

Delayed RNC interaction promotes non-native lamin dimer conformations

The above experiments showed that dimers of nascent lamin chains can be formed in situ but did not provide insight into unsuccessful assembly attempts or folding errors. We surmised the split FlAsH-tags may keep the N-termini connected after full unfolding, which could allow us to directly follow dimer formation and dissociation, including underlying conformational changes. Upon RNC coupling and FlAsH exposure, tethers indeed remained intact after lamin dimers were unfolded by stretching, as evidenced by a force drop to a non-zero level and the continued presence of the fluorescence signal (Fig. 2B). Note that the fluorescence signal is not visible at the lowest forces because the molecular tether may exit the confocal imaging plane. The force and fluorescence signals disappeared when the tether fully ruptured (broke), which could be due to FlAsH, Dig-AntiDig, uL4 or biotin-neutravidin dissociation, but whose rupture force should not depend on nascent chain length. Accordingly, we found similar rupture (or tether breaking) forces for all three constructs (Supplementary Fig. 7). In this manner, nascent chain dimers could be cyclically unfolded by stretching and then given a chance to reform by relaxation (Fig. 3A).

The measured forces and extensions (bead-to-bead distance) during the stretch-relax cycles report on the degree of nascent chain compaction. In principle, nascent chain compaction during relaxation and decompaction during stretching can reflect various underlying conformational changes. Details of the force-extension data can be used to distinguish these possibilities. For instance, a sudden and discrete increase in extension during stretching typically indicates an unfolding transition. In turn, this shows that a folded state had formed in the previous relaxed state. We note that the FlAsH moiety may not always bind, for instance, if the two coils would initially not be in register. Stretching would then lead to simple tether breakage, as we have observed in the absence of FlAsH (Fig. 1, Supplementary Fig. 7). Out-of-registry rupture and assembly therefore cannot be studied in higher detail with our method.

Four classes of behaviour were observed (Fig. 3B, Supplementary Fig. 8), with individual RNC pairs showing different classes from one cycle to the next (Supplementary Fig. 9). The chains were for the largest part either: (1) initially unfolded, and remaining so throughout the stretch-relax cycle, (2) initially compact and gradually decompacting during stretching (or conversely becoming gradually more compact during relaxation), with the data resembling previous pulling experiments on stretched linear α-helices[47,48], (3) initially compact and unfolding discretely, consistent with the formation and unfolding of the coiled-coil dimer[40] (see also Fig. 2B), or (4) initially compact and remaining so throughout the cycle, with the applied force unable to unfold the structure.

The compacted states (4) indicated the formation of stable non-native conformations that differ from coiled-coil or linear α-helical structures[49]. These states were preserved for multiple cycles until the tether ruptured, indicating that the nascent chains could no longer form coiled-coil-like dimers. Conversely, unfolded (1) and α-helix-like states (2) could transition at 0 pN to the coiled-coil-like state that unfolded in discrete steps (3) (Supplementary Fig. 9). In line with these data and the increased dimerization propensity with nascent chain length (Fig. 1D), class (3) was found to increase in frequency with nascent chain length, while classes (1) and (2) decreased (Fig. 3C). Notably, class (4) was only observed for the longest fragment (Fig. 3B, C, Supplementary Fig. 8). Note that these stretch-relax assays with different fragment lengths thus allow one to study the conformational consequences for nascent chains that start interacting during different phases of translation. Also note that unfolded polypeptides may be in different rotational states that can affect the ability to form secondary and tertiary structure. Overall, these data indicated that two neighbouring nascent chains can adopt α-helical and coiled-coil dimer structures early during translation, which grow as translation progresses. Alternatively, however, non-native states are promoted when the interactions between chains are delayed until later phases of translation.

Co-co assembly suppresses intra-chain lamin misfolding

A key question concerns the conformational competition that determines the different observed folding pathways. Native complex formation can be in competition with aggregation interactions between the chains, or misfolding interactions within chains—both of which could yield the observed non-native states (Fig. 3). To address this issue, we probed single ribosome-associated lamin nascent chains, in the absence of partnering RNCs (Fig. 4A). First, we generated stalled ribosomes tethered to beads via 5 kb DNA handles as before, using suppressor tRNAs to biotinylate the nascent chains N-terminally. After trapping one bead, the biotinylated nascent chain was linked to a second trapped bead via another 5 kb DNA handle. Next, we cyclically first separated and subsequently approached the two optical traps, thus stretching and relaxing the α-helical lamin rod domains by their N- and C-termini, for all three lamin fragments (Fig. 4A).

With single RNCs, we observed three of the four classes (Fig. 4B, C, Supplementary Fig. 10): (1) unfolded, (2) α-helix-like, and (4) non-native. As expected, observations of the discrete unfolding corresponding to the coiled-coil-like dimer class (3) were negligible. The data indicated that a second nascent chain is not required, but may promote α-helix formation. However, most notable was the prominence of the non-native class (4). This class was observed for all fragments, at frequencies ranging from 20% for the shortest to 60% for the longest (Fig. 4C), while for the RNC pairs it was detected for the longest fragment only, and at a low frequency of 20% (Fig. 3C). These data indicate that in the absence of another lamin nascent chain, the individual lamin nascent chains were prone to form compact and stable non-native structures. Indeed, polypeptides that can form α-helices can also form misfolds that have high contact-order and are hence compact[50]. Conversely, the presence of a second nascent chain suppressed this lamin misfolding while enabling the coiled-coil-like assembly. Hence, native structure formation here is not inhibited, but instead promoted by interactions between nascent polypeptide chains.

Ribosome pair asymmetry and proximity

We thus far paired two identical RNCs (Figs. 2 and 3) in order to study the interaction between two nascent chains in similar phases of translation. Alternatively, one ribosome may have translated substantially further than the other. To study this asymmetric scenario, we performed RNC pairing assays as before (Fig. 3), but now using one bead with an intermediate-fragment RNC ($LMNA_{31\text{-}311}$) and one bead with a long-fragment RNCs ($LMNA_{31\text{-}476}$). These conditions indeed produced tethers and showed the previously observed classes during stretch-relax experiments: (1) unfolded, (2) α-helix-like, (3) coiled-coil-like, and (4) non-native (Supplementary Fig. 11A, B). These data thus showed that asymmetric RNC pairs also can generate lamin dimers in vitro. The intermediate-long asymetric RNC pairs displayed a higher frequency of non-native cases than the symmetric intermediate RNC pairs, which did not show these states (Supplementary Fig. 11C). This is consistent, as the longer nascent chain of the leading ribosome provides more opportunities for non-native interactions. These experiments in vitro show that ribosomes being in similar phases of translation and in close proximity on the RNA message is not strictly required but may be beneficial for co-translational lamin dimerization.

It has been shown that ribosomes can favor unfolded over folded states of nascent chains[3]. A similar or even stronger effect might occur here, as two ribosomal surfaces are brought in close proximity to the lamin dimer when it forms co-translationally. To test the potential difference in lamin dimer stability on and off the ribosome, we purified lamin dimers of the intermediate construct, after engineering ybbR tags for DNA handle attachment, and performed similar single-molecule stretching and relaxation experiments in the absence of ribosomes (Supplementary Fig. 12). Strikingly, the purified dimers could not be unfolded even when stretched to the maximum force of 65 pN in our assay. While small unfolding events were observed, for the majority of curves they totaled less than 30 nm (Supplementary Fig. 12D). Such a destabilizing effect of ribosome proximity may be beneficial to co-co assembly, by allowing more options for finding the lowest-energy dimeric state.

Proteome-wide considerations

To assess the importance of interfacial contacts for co-translational dimer formation throughout the proteome, we analyzed the inter- and intra-molecular contacts of co-co candidates from our DiSP study[16] (Supplementary Fig. 13). We found that the relative abundance of inter- vs. intra-molecular contacts was similar for high and low confidence co-co assembling candidates (Supplementary Fig. 13A). Two peaks were observed: A first subpopulation of nascent dimers that showed over 10-fold more inter- than intra-chain contacts (15% of dimers), suggesting an important role for the partner chain in stabilization. Coiled-coils including lamin are very dependent on inter-chain contacts, as they rely solely on an α-helix structure for intra-chain stabilization. The second sub-population showed less than 10-fold more inter- than intra-chain contacts at co-co onset (85% of dimers), which could indicate partial domain folding before dimerization. Dimers in this group may also employ self-chaperoning, in particular dimers with an inter- vs. intra-chain contact ratio of more than 1. For most proteins, the inter-chain contacts were more important at the co-co assembly onset than after translation, when considering the total dimer interface (Supplementary Fig. 13C). This suggested that the stabilizing initial inter-chain contacts are further stabilized by intra-chain contacts later during translation. Thus, the self-chaperoning mechanism may be especially useful in early translation phases.

https://doi.org/10.1038/s41467-025-61500-y

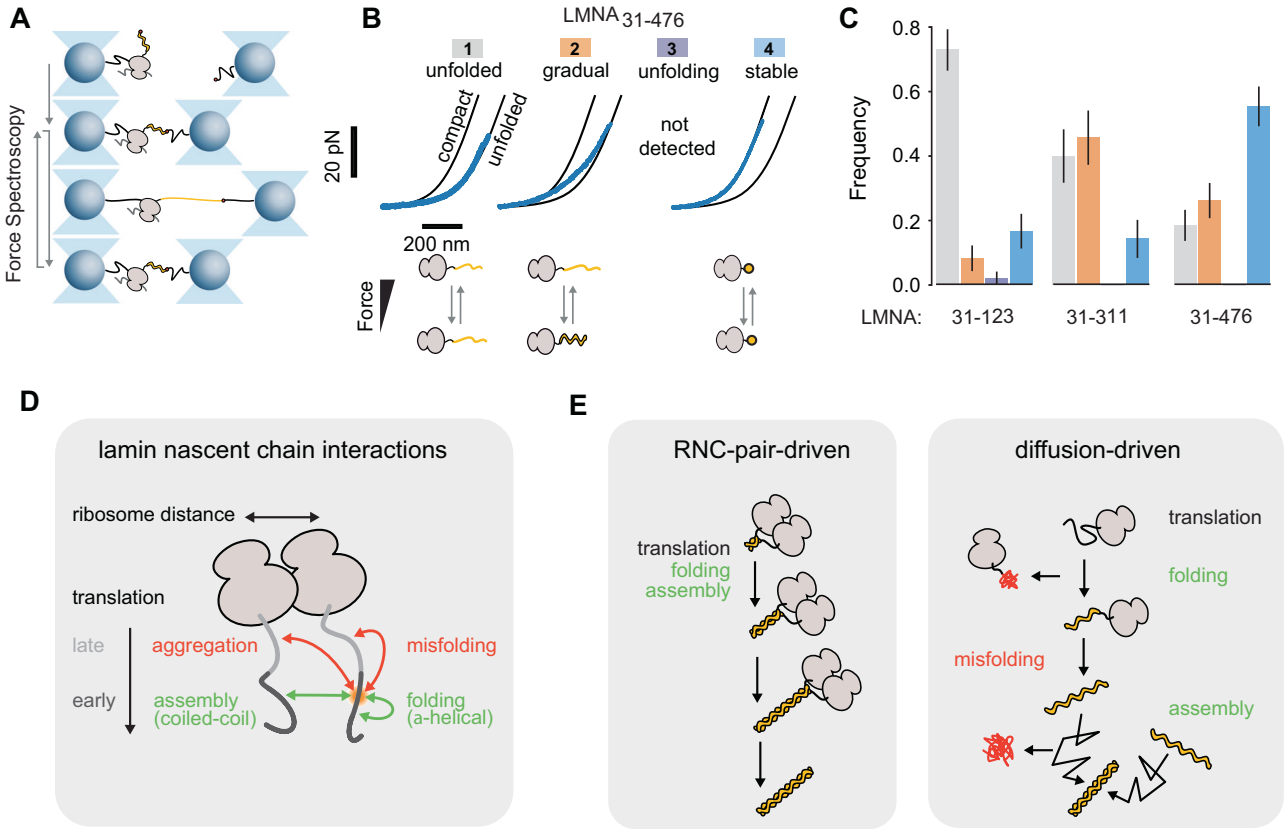

Fig. 4 | Lamin misfolds when interactions with other nascent chains are denied. **A** Diagram of optical tweezer approach to probe single monomeric lamin nascent chains. **B** Classes of observed force-extension behaviour for monomeric lamin nascent chains. Black lines: reference for a single nascent chain being compact (left) or fully unfolded (right). Four classes of conformational states are distinguished, with the majority of the chains: (1) remaining unfolded, (2) initially compact and extending gradually under tension, as expected for linear α-helices, (3) initially compact and unfolding discretely, typical for a dimer state that cannot form here, (4) initially compact and remaining so up to 45 pN, typically for multiple stretch-relax cycles, indicative of a kinetically trapped misfolded state. Data is shown for $LMNA_{31\text{-}476}$ fragments. **C** Frequency of stretch-relax cycles with specific force-extension features (see **B**), for lamin nascent chain monomers of three nascent chain lengths ($n = 14$ $LMNA_{31\text{-}123}$ molecules, 45 pulling cycles, $n = 13$ $LMNA_{31\text{-}311}$ molecules, 32 pulling cycles, $n = 17$ $LMNA_{31\text{-}476}$ molecules, 65 pulling cycles). $LMNA_{31\text{-}311}$ and $LMNA_{31\text{-}476}$ are significantly different ($p = 0.0003$, Chi^2-test). Error bars are standard error of proportion. **D** Competition between initial lamin nascent chain interactions and factors that affect it. A site (orange) can engage in non-native interactions (orange arrows), and native (α-helical) folding and (coiled-coil) assembly (green arrows). The coils natively contact 'in-register' early in translation. Delayed interactions causes more competition from 'out-of-register' interactions. Larger ribosome distances inhibit the stabilizing assembly interactions and promotes intra-chain misfolding interactions. **E** Schematic of ribosome-pair and diffusion-driven assembly. The former promotes proper folding and assembly by establishing native inter-chain contacts before non-native intra-chain contacts can form, and by limiting cytosolic exposure. Source data are provided as a Source Data file. RNC cartoon from Bertolini et al.[16]. Reprinted with permission from AAAS.

Discussion

In this study, we report that by coupling co-translationally, RNC pairs can drive the assembly of coiled-coil homodimers composed of subunits that misfold in isolation. We find that physical RNC proximity and their translation progress along the mRNA biases the competition between native and non-native contacts, which both can form within single chains or between two chains (Fig. 4D, Supplementary Fig. 14). Specifically, residues that are translated early can form non-native contacts with chain segments that are translated later (Fig. 4D, red arrows), which compete with native coiled-coil contacts (Fig. 4D, green arrows). Timely formation of the latter native contacts between nascent chains allows the realization of partial coiled-coils, which grow in size and stability as translation proceeds (Fig. 4E). Conversely, non-native contacts are promoted when the RNCs either cannot interact, or interaction is delayed until later phases of translation. Lamin nascent chains then misfold and are no longer assembly-competent (Fig. 4B, C). These risks should be further aggravated when assembly is postponed until after translation, and the monomeric lamin subunits must diffuse through the cytosol in order to dimerize (Fig. 4F). Overall, nascent chain interactions during translation thus provide a reciprocal chaperoning function that suppresses misfolding, in contrast with the view that high local nascent chains concentrations promote aggregation[51].

The ability to synthesise complexes composed of misfolding-prone subunits may be of broad relevance to cells, as it expands the range of possible protein structures and functions. Indeed, the elongated lamin shape renders the lamin subunits prone to misfolding in monomeric form, yet is also key to its unique mechanical properties[52]. The early and co-translational lamin dimerization we observed may be relevant to efficient subsequent import into the nucleus, where lamin dimers polymerize[53]. Importin-α, which binds the lamin nuclear localization signal and can inhibit premature polymerization[54], may hence provide co- and post-translational lamin chaperoning functions. Lamina-associated polypeptide 2α (LAP2α) may also help to maintain a soluble pool of lamin dimers in the cytosol[53].

Coupled folding and assembly by RNC pairs can impact other translational processes. For instance, peptide bond formation and translational pausing are known to be affected by co-translational folding and related generated pulling forces in the order of 10 pN[55–57], and may similarly be controlled by co-translational assembly transitions. While our data do not directly show the forces generated by lamin dimerization, the dimer disruption forces we measured (several

tens of pN) are of similar order as co-translational folding events[3,58], which suggests that they are large enough to modulate translational activity.

The mechanism we report is likely more widely relevant, given the recently observed prevalence of RNC pairing for coiled-coil and other homodimer classes, including BTB and Rel homology domain proteins[16], and may extend to heterodimers, higher-order oligomers, as well as membrane-based biogenesis. For instance, it is an interesting question whether intermediate filaments with a heterodimeric coiled-coil structure also assemble co-translationally in *trans*, thus involving two rather than one mRNA strand, and hence rely on the self-chaperoning mechanism we report. Our mechanism may thus contribute to understanding the architecture and (mutation-induced) misfolding of proteins ranging from intermediate filaments to major regulatory and metabolic proteins such as initiation factor 2B and Fatty Acid Synthase. Furthermore, the findings raise the question of whether the formation and translation synchrony of RNC pairs is controlled. The latter may be achieved by sequence-induced translational pausing or regulatory factors, as recently studied in ribosome collision detection[59]. Finally, the results may open up new routes in artificial protein and mRNA therapy design.

Methods

Disome selective profiling (DiSP)

U2OS (ATCC Cat# HTB-96, RRID: CVCL_0042) and HEK293-T cells (DSMZ Cat# ACC 635) were cultivated in high glucose DMEM media containing GlutaMAX and pyruvate (Gibco), which was freshly supplemented with 10% heat-inactivated FCS (Gibco), 100 U/mL penicillin and 100 µg/mL streptomycin (Gibco) and were grown in a humidified incubator with 5% CO_2 at 37 °C (HERAcell 150i). Variations in the lysis protocol were implemented in different datasets. A lysis buffer with physiological salt concentration (50 mM HEPES pH 7.0, 10 mM $MgCl_2$, 150 mM KCl, 1% NP40, 10 mM DTT, 100 µg/ml CHX, 25 U/ml recombinant Dnase1 (Roche) and protease inhibitor (complete EDTA free, Roche)) was used for DiSP of HEK293-T and U2OS cells (Supplementary Fig. 2A, D). A high-salt lysis buffer containing 500 mM KCl was employed for DiSP of HEK293-T cells to test possible effects on the detected onset of lamin disome formation (Fig. 1B). DiSP of U2OS cells was also performed by lysing cells in the presence of chemical crosslinkers (Supplementary Fig. 2C). In this case, the lysis buffer was supplemented with 2.5 mM BS3 and 20 mM EDC. Cells were scraped in crosslinker-containing lysis buffer on ice, such that crosslinking occurred simultaneously with cell lysis. After lysis, DiSP samples were processed[16]. Briefly, clarified cell lysates were loaded on sucrose gradients (5% - 45%), centrifuged for 3.5 h at 150,000 × *g* 4 °C (SW40-rotor, Sorvall Discovery 100SE Ultracentrifuge) and fractions corresponding to the monosome and disome peaks were collected. 30 nt long footprints were extracted from both monosome and disome fractions and deep sequenced. DiSP gene density profiles show the position-wise 95% Poisson confidence interval corrected for library size, and read counts are smoothed with a 15-codon wide sliding window[16].

Cloning

All primer sequences used for cloning are available in Supplementary Table 1. *LMNA* corresponding to lamin C that lacks the unstructured head domain (residues 31–542), was PCR-amplified from a self-made U2OS cDNA library (SuperScript™ III first-strand synthesis kit, ThermoFisher). The employed PCR primers (MB143 + MB144) added an NdeI restriction site followed by a splitFlAsH tag (SF: MAGSCCGG) at the 5′ end and a TwinStrep tag (TS: GGSGSAWSHPQFEKGG GSGGGSGGSAWSHPQFEKGA) with a BamHI overhang at the 3′ end of the construct (final sequence named SF-LMNC-TS). T4 DNA ligase was used to ligate the gel-purified PCR fragment into a BamHI/NdeI-restricted pET3a vector. The resulting plasmid was confirmed by Sanger sequencing. Fragments for Gibson assembly were generated by PCR reactions on the SF-LMNC-TS amplicon (described above) using the primer combinations JS9 and JS10, JS9 and JS11, JS9 and JS12. Primers JS7 and JS8 were used to create the linear pRSET plasmid backbone, containing the SecMstrong sequence (FSTPVWIWWWPRIRGPP) at the 5′ end and the T7 promoter at the 3′ end. The *LMNA*-containing fragments were assembled with the linear plasmid backbone by Gibson assembly. Plasmids were isolated using standard procedures and confirmed by Sanger sequencing. From these plasmids, the linear dsDNA templates for the in vitro transcription/translation reaction were amplified by PCR using primers JS28 and JS29.

Plasmids for post-translational lamin constructs (pJS81, pJS82) were cloned using homology-based in vivo DNA assembly[60]. The pET3a backbone was linearized from stop to start by PCR using oligos JS169 and JS170. N-terminal extensions (M-HHHHHH-AGS-C/CC-GG) were added via primers JS315 (single Cys) or JS316 (double Cys), respectively, and the C-terminal ybbR-tag was introduced with JS318. After DpnI digestion, *Escherichia coli* XL1 cells were transformed with backbone and insert for in vivo assembly. Plasmids were selected on ampicillin-containing LB plates and confirmed by Sanger sequencing.

Purification of post-translational lamin constructs

BL21(DE3) + pRare (Cam^R) cells containing pJS81 (Amp^R) or pJS82 (Amp^R), respectively, were grown at 30 °C in 1 L 2xYT medium supplemented with 100 µg/mL ampicillin and 5 µg/mL chloramphenicol. When the OD_{600} reached 1, expression was induced with 1 mM IPTG for 4 hours. Cells were harvested by centrifugation at 4 °C, 4000 rcf for 15 min and snap-frozen in liquid nitrogen. The pellet was resuspended in lysis buffer (50 mM HEPES-KOH pH 7.5, 150 mM KCl, 5% (v/v) glycerol, cOmplete EDTA-free protease inhibitor cocktail (Roche)) to ~100 OD/mL and lysed in a French pressure cell press at ~16,000 PSI. The lysate was clarified by centrifugation at 4 °C, 30,000 rcf for 30 min. The supernatant was loaded onto a Protino Ni-NTA Agarose (MACHEREY-NAGEL) gravity flow column, washed (25 mM HEPES-KOH pH 7.5, 500 mM KCl, 5% (v/v) glycerol) and eluted (25 mM HEPES-KOH pH 7.5, 150 mM KCl, 5% (v/v) glycerol, 250 mM Imidazole pH 8.0). The sample was concentrated with a centrifugal filter (MWCO 5 kDa) and dimers were isolated by size-exclusion chromatography (Äkta Superdex 200 pg) using coupling buffer (50 mM HEPES-KOH pH 7.5, 10 mM $MgCl_2$, 5% (v/v) glycerol). Pooled dimeric fractions were concentrated again and snap-frozen in liquid nitrogen.

Attachment of DNA handles to purified lamin dimers

Purified His-CC-LMNA31-311-ybbR protein was coupled to 20 nt oligo (Supplementary Table 1) modified with CoA (Biomers GmbH) in the presence of 50 mM HEPES, 10 mM MgCl2 (both Merck) and 1 µM SFP synthase (addgene) at 4 °C overnight. The remaining oligos were removed by Ni-NTA purification (Protino, MACHEREY-NAGEL). The 1.3 kb DNA handles were created by PCR amplification from pUC19 plasmid (New England Biolabs) using primers modified with phosphate on one end and either biotin or digoxigenin on the other end (Eurofins, Germany). The DNA fragment was purified using Qiagen PCR Purification Kit (Qiagen). The DNA was subsequently digested with Lambda exonuclease (New England Biolabs) at 37 °C for 2 h, followed by 10 min inactivation at 75 °C. Obtained ssDNA was purified with an Amicon 30 kDa column (Merck, Darmstadt, Germany). The second strand was completed using Deep Vent (exo-) DNA polymerase (New England Biolabs), dNTP mix (ThermoFisher) and a phosphorylated primer (Eurofins, Germany) starting 20 nt downstream to create the overhang. The final product was purified using PCR purification Kit (Monarch). The 1.3 kb DNA handles with 20 nt overhang complementary to the oligo attached to protein and biotin or digoxigenin was ligated to protein-oligo complex using T4 ligase (New England Biolabs) at 16 °C for 4 h followed by overnight incubation on ice. The resulting DNA-LaminDimer-DNA complex was flash-frozen and stored at −80 °C for future analysis.

Coupling of neutravidin-DNA handles to beads

Double-stranded DNA (dsDNA) molecules were prepared by PCR amplification using digoxigenin (DIG) and biotin 5'-end-modified primers (Supplementary Table 1). 2DIGfw5kbp and 3BIOrev5kbp were used with pOSIP-TT as a template in a two-step Phire Green Hot Start II PCR (Thermo Scientific) reaction. The 5 kb PCR product was purified using the QIAquick PCR Purification Kit (QIAGEN). 10 nM 5 kb DNA was coupled to 2 µM neutravidin (Thermo Scientific) by incubation in 10 mM PBS overnight at 4 °C. 2.1 µm diameter carboxyl-functionalized polystyrene beads (Spherotech) were modified with anti-digoxigenin (anti-DIG, Roche), using the carbodiimide crosslinker EDAC, following the PolyLink protein coupling kit protocol (Polysciences). Subsequently, the resulting 5 kb neutravidin-DNA handles (1.7 µm contour length) were coupled to the anti-DIG beads at a reaction ratio of ~10 neutravidin-DNA/bead for 30 min at 4 °C. The beads with the neutravidin-DNA handles were then washed several times with Tico buffer (20 mM HEPES-KOH pH 7.6, 10 mM $(Ac)_2Mg$, 30 mM $AcNH_4$, 4 mM β-mercaptoethanol) and split into two batches (modified protocol from ref. 61).

Ribosomes from an RNase-deficient *E. coli* K-12 strain (Can20/12E[62]) were biotinylated in vivo at the uL4 ribosomal protein and subsequently isolated[17]. Biotinylated ribosomes were added to one batch of Tico-washed neutravidin-DNA modified beads at 350 nM, supplemented with murine RNase inhibitor (New England Biolabs) and incubated at 4 °C for 30 min. The remaining unbound ribosomes were then removed via pelleting and the beads were washed once with Tico buffer before they were resuspended directly into the cell-free transcription/translation mix described below.

Cell-free protein synthesis and co-translational labelling

The cell-free transcription/translation mix used in this study is a customized version of the bacterial PURE system without ribosomes (PURExpress Δ ribosomes, New England Biolabs). Biotin was incorporated co-translationally at the two N-terminal amber positions TAG using the suppressor tRNA technique[17]. The system was supplemented with 10 µM of a modified tRNA pre-charged with biotinylated lysine (Biotin-XX-AF_tRNA, amber, CloverDirect), 0.5-5 µM trigger factor, as well as murine RNase inhibitor (New England Biolabs). Synthesis was initiated by mixing the system with the *E. coli* ribosomes coupled to beads, and the 5.5 nM linear DNA template. The reaction mixture was incubated at 37 °C for 30 min. The resulting nascent chains remained attached to the ribosome due to the SecMstr arrest peptide at the C-terminus[32,63]. Following the transcription/translation reaction, the bead with their tethered and stalled ribosome nascent chain complexes (RNCs) were resuspended in TICO buffer (20 mM HEPES-KOH pH 7.6, 10 mM $(Ac)_2Mg$, 30 mM $AcNH_4$, 4 mM β-mercaptoethanol) at 4 °C. The RNC-coupled beads were diluted in 300 µL TICO buffer prior to their usage in the optical tweezers. As oxygen scavenger the P2O system (3 units per ml pyranose oxidase, 90 units per ml catalase and 50 mM glucose, Sigma) was used.

Preparation of the FlAsH dye

Stock solutions of 5 mM were prepared by dissolving FlAsH-EDT_2 (Carbosynth) in DMSO (Thermo Scientific) and stored in an inert atmosphere at −20 °C. For experimental use, the stock solutions were diluted in TICO buffer to a working concentration of 100 nM.

Optical tweezers assay and single-molecule data analysis

Correlated single-molecule force spectroscopy and multi-color confocal laser scanning spectroscopy measurements were carried out with the C-trap instrument (Lumicks, Amsterdam). This instrument features two optical traps formed by a high-intensity and polarization-stable single 1064 nm laser, which is split into two orthogonally polarized beams, one of which can be steered with a piezo mirror relative to the other. Two fluorescence excitation lasers (532 nm and 638 nm) allow for dual color confocal fluorescence, while the dedicated APDs assure single-photon sensitivity. Measurements were performed in a monolithic laminar flow cell with a stable passive pressure-driven microfluidic system with 5 separate flow channels. Data was acquired at a rate of 50 kHz, decimated/averaged down to 500 Hz, and was analysed using custom scripts in Matlab and python. Calibration of the two orthogonally polarized traps was performed using the power spectrum method, where the power spectra obtained from the beads undergoing Brownian motion in the optical traps are fitted with a Lorentzian to obtain conversion parameters for displacements and forces in nm and pN[64]. The trapping laser intensity was kept constant for all measurements, resulting in a trap stiffness of about 260 ± 50 pN/µm. To tether individual molecules, the optically trapped beads were brought within close proximity for short time intervals, before separating them to an inter-bead distance of about 3 µm. A slight increase in the force would signal tether formation. Measurements were taken in a cycling force spectroscopy mode, where the steerable trap was moved at a constant rate of 0.2 µm/s between a minimum bead separation of 2 µm and a maximum force of up to 65 pN. The resulting force-extension curves for individual tethers were fitted with two worm-like chains (WLC) in series, one for the DNA handle contribution (extensible worm-like chain, eWLC)[65] and the other for the stalled nascent chain contribution (inextensible worm-like chain, WLC)[66], yielding an average DNA persistence length of 43 ± 10 nm (SD of 5 nm) and a DNA stretch modulus of 1037 ± 388 pN/nm (SD of 194 pN/nm). Tethered molecules undergoing only gradual transitions could not be fitted with the Odijk inextensible approximation WLC model, and hence WLC rulers were used corresponding to fully compacted and fully extended monomer and dimer chains as depicted in Figs. 3B and 4B, and Supplementary Figs. 4 and 8–12 using the average DNA parameters obtained above. Four features were identified during the pulling-relaxation experiments of monomers and dimers. Most of the total chain was characterized as: (i) unfolded, (ii) extending or compacting gradually, (iii) compacted and unfolding in discrete events, and (iv) compacted and not unfoldable. More specifically, the features were: (i) An unfolded state, in which more than half of the total monomer or dimer chain is unfolded, and remains so during a stretch-relax cycle. (ii) A compacted (or an extended) state composed of more than half of the total monomer or dimer chain, which displayed a gradual contour length increase (decrease) of more than half of the total chain length during a stretch-relax cycle. (iii) A compacted state composed of more than half of the total monomer or dimer chain, which displayed multiple discrete contour length changes totalling more than half of the total chain length during a stretch-relax cycle. (iv) A compacted state composed of more than half of the total monomer or dimer chain, which displayed no detectable contour length change during a stretch-relax cycle.

Estimation of lamin dimer stability

To assess the dimer stability of our constructs, we considered the following. Coiled-coil interactions involve heptad repeats $(abcdefg)_n$ in both monomers. Residues a and d are predominantly hydrophobic and make up the core of the coiled-coil interface, while e and g are typically charged or polar and occupy the region between the core and the solvent. (Supplementary Fig. 5A). Structural stability is affected by the number of heptad repeats and the side chain packing at position a and d, with Leucine, Valine and Isoleucine most commonly observed at these positions[36,38,67,68]. The packing is affected by van der Waals interactions between side chains, for instance[69]. The packing arrangement for coiled coils is termed knobs-into-holes (KIH) (Supplementary Fig. 5C). A 'knob' is defined as a side chain of position a and d residues that project from one helix and packs into a diamond-shaped 'hole' formed by four side chains of an adjacent helix. Three of the four residues of this diamond are themselves knobs, so that a complementary interlocking structure results[34,35]. The *a* sites can

accommodate more residue types than *d*, including the bulkier β-branched amino acids, like Val and Ile. The inward pointing orientation of the side chain at the d position is thought to best accommodate amino acids which are not branched at the β-carbon[36–38]. Side-chain mobility contributes significantly to the stability of the folded state. The number of side chain rotamers, can be an additional source of stability[70].

Hence, we counted the full heptads (abcdefg) for each construct and considered the a and d amino acid. Construct 2 has 15 more heptads than construct 1 (of which 5 had Val, Ile or Leu at site a and d, Supplementary Fig. 5B). In contrast, construct 3 gains only 7 more full heptads compared to construct 2 (with less ideal amino acids at site a and d). Thus, we predict that construct 2 is significantly more stable than construct 1, while construct 3 is only slightly more stable than construct 2. Consistently, the calorimetric enthalpy of coil 1B (in construct 2 and 3) was measured as above 55 kcal/mol, while 2B (fully present only in construct 3) showed a smaller ~3.7 kcal/mol[71]. These values agree with our mean rupture forces, which double from construct 1 (~7pN) to construct 2 (~14pN), but increase only marginally to construct 3 (18pN, *p*-value: 0.5).

Next, we calculated inter-chain energies. Because side chains are key to the interactions, we used side chain centroids to represent the residues. Residues were considered in contact if their centroids were closer than 6.5 Å, using Alphafold2 for structure prediction (Supplementary Fig. 5D, E). Cumulative effective contact energies were determined using the approach by Zhang C. et al.[39]. Consistent with the above estimates and our data, the largest energy drop is seen from construct 1 to construct 2 (Supplementary Fig. 5F).

One may note the regions with few contacts (marked in pink, Supplementary Fig. 5D–F), which link the coils and hendecad patterns (abcdefghijk). The hendecad region in coil 1B (res 207–277) forms an untwisted helical section (Supplementary Fig. 5D), which gives rise to mismatched inter-helical hydrophobic interactions and therefore to fewer contacts[67]. The fewer contacts within these regions are also reflected in plateaus within the cumulative contact energies plot (Supplementary Fig. 5F).

Calculation of all-atom inter- and intra-molecular contacts for proteome-wide co-co assembly candidates

Initial structures of complexes were selected by aligning the amino acid sequences of high and low confidence co-co candidates to every protein chain larger than 25 amino acids from the PDB (January 3rd, 2023) using adlib (https://pypi.org/project/edlib/). Structural assemblies were a co-co candidate had at least 90% sequence similarity with at least two protein chains were kept ($n = 503$ for low-confidence and 95 for high-confidence genes, respectively). Then pair-wise permutated interfaces between protein chains were calculated. Interface contacts were defined as atom pairs of residues from different protein chains that had a distance of less than or equal to 5 Å. For these interface residues, intra-molecular chain contacts were calculated. These stabilizing contacts were defined as atom pairs of different residues from the same protein chain that had a distance of less than or equal to 5 Å and were at least 10 amino acids apart on the protein chain. Only inter- and intra-molecular contacts where both residues are emerged from the ribosomal exit tunnel at the co-co onset (30 amino acids before the co-co onset position) are considered and summed. Finally, the ratio between ribosome exposed inter- and intra-molecular contacts for every chain is calculated. Then the ratios of all chains from a co-co candidate were averaged by the median.

Reporting summary

Further information on research design is available in the Nature Portfolio Reporting Summary linked to this article.

Data availability

The sequencing data discussed in this publication have been deposited in NCBI's Gene Expression Omnibus and are accessible through GEO Series accession number GSE282964. Source data are provided with this paper.

Code availability

Data analysis of ribosome profiling datasets were performed with RiboSeqTools[16] (available at https://github.com/ilia-kats/RiboSeqTools). Other relevant custom codes used in this work have been deposited at zenodo/github [https://doi.org/10.5281/zenodo.15184282].

References

1. Junker, J. P., Ziegler, F. & Rief, M. Ligand-dependent equilibrium fluctuations of single calmodulin molecules. *Science* **323**, 5914 (2009).
2. Dill, K. A. & MacCallum, J. L. The protein-folding problem, 50 years on. *Science* **338**, 1042–1046 (2012).
3. Kaiser, C. M., Goldman, D. H., Chodera, J. D., Tinoco, I. Jr. & Bustamante, C. The ribosome modulates nascent protein folding. *Science* **334**, 1723–1727 (2011).
4. Phillip, Y. & Schreiber, G. Formation of protein complexes in crowded environments-from in vitro to in vivo. *FEBS Lett.* **587**, 1046–1052 (2013).
5. De Simone, A. et al. Intrinsic disorder modulates protein self-assembly and aggregation. *Proc. Natl. Acad. Sci. USA* **109**, 6951–6956 (2012).
6. Halbach, A. et al. Cotranslational assembly of the yeast SET1C histone methyltransferase complex. *EMBO J.* **28**, 2959–2970 (2009).
7. Shiber, A. et al. Cotranslational assembly of protein complexes in eukaryotes revealed by ribosome profiling. *Nature* **561**, 268–272 (2018).
8. Shieh, Y.-W. et al. Operon structure and cotranslational subunit association direct protein assembly in bacteria. *Science* **350**, 678–680 (2015).
9. Wells, J. N., Bergendahl, L. T. & Marsh, J. A. Operon gene order is optimized for ordered protein complex assembly. *Cell Rep.* **14**, 679–685 (2016).
10. Williams, N. K. & Dichtl, B. Co-translational control of protein complex formation: a fundamental pathway of cellular organization?. *Biochem. Soc. Trans.* **46**, 197–206 (2018).
11. Duncan, C. D. & Mata, J. Widespread cotranslational formation of protein complexes. *PLoS Genet.* **7**, e1002398 (2011).
12. Kamenova, I. et al. Co-translational assembly of mammalian nuclear multisubunit complexes. *Nat. Commun.* **10**, 1740 (2019).
13. Lin, L., DeMartino, G. N. & Greene, W. C. Cotranslational dimerization of the Rel homology domain of NF-kappaB1 generates -p105 heterodimers and is required for effective p50 production. *EMBO J.* **19**, 50–4722 (2000).
14. Nicholls, C. D., McLure, K. G., Shields, M. A. & Lee, P. W. Biogenesis of p53 involves cotranslational dimerization of monomers and posttranslational dimerization of dimers. Implications on the dominant negative effect. *J. Biol. Chem.* **277**, 12937–12945 (2002).
15. Redick, S. D. & Schwarzbauer, J. E. Rapid intracellular assembly of tenascin hexabrachions suggests a novel cotranslational process. *J. Cell Sci.* **108**, 1761–1769 (1995).
16. Bertolini, M. et al. Interactions between nascent proteins translated by adjacent ribosomes drive homomer assembly. *Science* **371**, 57–64 (2021).
17. Wruck, F., Katranidis, A., Nierhaus, K. H., Büldt, G. & Hegner, M. Translation and folding of single proteins in real time. *Proc. Natl. Acad. Sci.* **114**, 4399 (2017).
18. Holtkamp, W. et al. Cotranslational protein folding on the ribosome monitored in real time. *Science* **350**, 1104–1107 (2015).

19. McKeon, F. D., Kirschner, M. W. & Caput, D. Homologies in both primary and secondary structure between nuclear envelope and intermediate filament proteins. *Nature* **319**, 463–468 (1986).
20. van Steensel, B. & Belmont, A. S. Lamina-associated domains: links with chromosome architecture, heterochromatin, and gene repression. *Cell* **169**, 780–791 (2017).
21. Worman, H. J. & Bonne, G. "Laminopathies": a wide spectrum of human diseases. *Exp. Cell Res* **313**, 2121–2133 (2007).
22. Fisher, D. Z., Chaudhary, N. & Blobel, G. cDNA sequencing of nuclear lamins A and C reveals primary and secondary structural homology to intermediate filament proteins. *Proc. Natl Acad. Sci. USA* **83**, 6450–6454 (1986).
23. Weber, K., Plessmann, U. & Traub, P. Maturation of nuclear lamin A involves a specific carboxy-terminal trimming, which removes the polyisoprenylation site from the precursor; implications for the structure of the nuclear lamina. *FEBS Lett.* **257**, 411–414 (1989).
24. Sinensky, M. et al. The processing pathway of prelamin A. *J. Cell Sci.* **107**, 61–67 (1994).
25. Herrmann, H., Bar, H., Kreplak, L., Strelkov, S. V. & Aebi, U. Intermediate filaments: from cell architecture to nanomechanics. *Nat. Rev. Mol. cell Biol.* **8**, 562–573 (2007).
26. Stuurman, N., Heins, S. & Aebi, U. Nuclear lamins: their structure, assembly, and interactions. *J. Struct. Biol.* **122**, 42–66 (1998).
27. Dechat, T. et al. Nuclear lamins: major factors in the structural organization and function of the nucleus and chromatin. *Genes Dev.* **22**, 832–853 (2008).
28. Kolb, T., Maass, K., Hergt, M., Aebi, U. & Herrmann, H. Lamin A and lamin C form homodimers and coexist in higher complex forms both in the nucleoplasmic fraction and in the lamina of cultured human cells. *Nucleus* **2**, 425–433 (2011).
29. Ye, Q. & Worman, H. J. Protein-protein interactions between human nuclear lamins expressed in yeast. *Exp. Cell Res* **219**, 292–298 (1995).
30. Miller, O. L. Jr., Hamkalo, B. A. & Thomas, C. A. Jr. Visualization of bacterial genes in action. *Science* **169**, 392–395 (1970).
31. Brandt, F. et al. The native 3D organization of bacterial polysomes. *Cell* **136**, 261–271 (2009).
32. Cymer, F., Hedman, R., Ismail, N. & von Heijne, G. Exploration of the arrest peptide sequence space reveals arrest-enhanced variants. *J. Biol. Chem.* **290**, 10208–10215 (2015).
33. Xi, Z., Gao, Y., Sirinakis, G., Guo, H. & Zhang, Y. Single-molecule observation of helix staggering, sliding, and coiled coil misfolding. *Proc. Natl Acad. Sci. USA* **109**, 5711–5716 (2012).
34. Kumar, P. & Woolfson, D. N. Socket2: a program for locating, visualizing and analyzing coiled-coil interfaces in protein structures. *Bioinformatics* **37**, 4575–4577 (2021).
35. Walshaw, J. & Woolfson, D. N. Socket: a program for identifying and analysing coiled-coil motifs within protein structures. *J. Mol. Biol.* **307**, 1427–1450 (2001).
36. Woolfson, D. N. Understanding a protein fold: the physics, chemistry, and biology of alpha-helical coiled coils. *J. Biol. Chem.* **299**, 104579 (2023).
37. Zhu, B. Y., Zhou, N. E., Kay, C. M. & Hodges, R. S. Packing and hydrophobicity effects on protein folding and stability: effects of beta-branched amino acids, valine and isoleucine, on the formation and stability of two-stranded alpha-helical coiled coils/leucine zippers. *Protein Sci.* **2**, 383–394 (1993).
38. Yu, Y. B. Coiled-coils: stability, specificity, and drug delivery potential. *Adv. Drug Deliv. Rev.* **54**, 1113–1129 (2002).
39. Zhang, C. & Kim, S. H. Environment-dependent residue contact energies for proteins. *Proc. Natl. Acad. Sci. USA* **97**, 2550–2555 (2000).
40. Bornschlogl, T. & Rief, M. Single-molecule dynamics of mechanical coiled-coil unzipping. *Langmuir* **24**, 1338–1342 (2008).
41. Bornschlogl, T. & Rief, M. Single molecule unzipping of coiled coils: sequence resolved stability profiles. *Phys. Rev. Lett.* **96**, 118102 (2006).
42. Goktas, M. et al. Molecular mechanics of coiled coils loaded in the shear geometry. *Chem. Sci.* **9**, 4610–4621 (2018).
43. Ramm, B. et al. Sequence-resolved free energy profiles of stress-bearing vimentin intermediate filaments. *Proc. Natl Acad. Sci. USA* **111**, 11359–11364 (2014).
44. Sadeghi, S. & Emberly, E. Length-dependent force characteristics of coiled coils. *Phys. Rev. E Stat. Nonlin Soft Matter Phys.* **80**, 061909 (2009).
45. Lopez-Garcia, P. et al. Structural determinants of coiled coil mechanics. *Phys. Chem. Chem. Phys.* **21**, 9145–9149 (2019).
46. Luedtke, N. W., Dexter, R. J., Fried, D. B. & Schepartz, A. Surveying polypeptide and protein domain conformation and association with FlAsH and ReAsH. *Nat. Chem. Biol.* **3**, 779–784 (2007).
47. Wolny, M. et al. Stable single α-helices are constant force springs in proteins. *J. Biol. Chem.* **289**, 27825–27835 (2014).
48. Schwaiger, I., Sattler, C., Hostetter, D. R. & Rief, M. The myosin coiled-coil is a truly elastic protein structure. *Nat. Mater.* **1**, 232–235 (2002).
49. Bechtluft, P. et al. Direct observation of chaperone-induced changes in a protein folding pathway. *Science* **318**, 1458–1461 (2007).
50. Lin, M. M., Shorokhov, D. & Zewail, A. H. Dominance of misfolded intermediates in the dynamics of alpha-helix folding. *Proc. Natl. Acad. Sci. USA* **111**, 14424–14429 (2014).
51. Natan, E. et al. Cotranslational protein assembly imposes evolutionary constraints on homomeric proteins. *Nat. Struct. Mol. Biol.* **25**, 279–288 (2018).
52. Elzeneini, E. & Wickstrom, S. A. Lipodystrophic laminopathy: Lamin A mutation relaxes chromatin architecture to impair adipogenesis. *J. Cell Biol.* **216**, 2607–2610 (2017).
53. Buchwalter, A. Intermediate, but not average: The unusual lives of the nuclear lamin proteins. *Curr. Opin. Cell Biol.* **84**, 102220 (2023).
54. Adam, S. A., Sengupta, K. & Goldman, R. D. Regulation of nuclear lamin polymerization by importin alpha. *J. Biol. Chem.* **283**, 8462–8468 (2008).
55. Ismail, N., Hedman, R., Schiller, N. & von Heijne, G. A biphasic pulling force acts on transmembrane helices during translocon-mediated membrane integration. *Nat. Struct. Mol. Biol.* **19**, 1018–1022 (2012).
56. Fritch, B. et al. Origins of the mechanochemical coupling of peptide bond formation to protein synthesis. *J. Am. Chem. Soc.* **140**, 5077–5087 (2018).
57. Goldman, D. H. et al. Ribosome: mechanical force releases nascent chain-mediated ribosome arrest in vitro and in vivo. *Science* **348**, 457–460 (2015).
58. Wruck, F. et al. The ribosome modulates folding inside the ribosomal exit tunnel. *Commun. Biol.* **4**, 523 (2021).
59. Cerullo, F. et al. Bacterial ribosome collision sensing by a MutS DNA repair ATPase paralogue. *Nature* **603**, 509–514 (2022).
60. Watson, J. F. & Garcia-Nafria, J. In vivo DNA assembly using common laboratory bacteria: A re-emerging tool to simplify molecular cloning. *J. Biol. Chem.* **294**, 15271–15281 (2019).
61. Jadhav, V. S., Bruggemann, D., Wruck, F. & Hegner, M. Single-molecule mechanics of protein-labelled DNA handles. *Beilstein J. Nanotechnol* **7**, 138–148 (2016).
62. Zaniewski, R., Petkaitis, E. & Deutscher, M. P. A multiple mutant of Escherichia coli lacking the exoribonucleases RNase II, RNase D, and RNase BN. *J. Biol. Chem.* **259**, 11651–11653 (1984).
63. Kempf, N. et al. A novel method to evaluate ribosomal performance in cell-free protein synthesis systems. *Sci. Rep.* **7**, 46753 (2017).
64. Berg-Sorensen, K. & Flyvbjerg, H. Power spectrum analysis for optical tweezers. *Rev. Sci. Instrum.* **75**, 594–612 (2004).

65. Hegner, M., Smith, S. B. & Bustamante, C. Polymerization and mechanical properties of single RecA-DNA filaments. *Proc. Natl Acad. Sci. USA* **96**, 10109–10114 (1999).
66. Odijk, T. Stiff chains and filaments under tension. *Macromolecules* **28**, 7016–7018 (1995).
67. Ahn, J. et al. Structural basis for lamin assembly at the molecular level. *Nat. Commun.* **10**, 3757 (2019).
68. Keating, A. E., Malashkevich, V. N., Tidor, B. & Kim, P. S. Side-chain repacking calculations for predicting structures and stabilities of heterodimeric coiled coils. *Proc. Natl Acad. Sci. USA* **98**, 14825–14830 (2001).
69. Moitra, J., Szilak, L., Krylov, D. & Vinson, C. Leucine is the most stabilizing aliphatic amino acid in the d position of a dimeric leucine zipper coiled coil. *Biochemistry* **36**, 12567–12573 (1997).
70. Bruce Yu, Y., Lavigne, P., Privalov. P. L. & Hodges, R. S. The measure of interior disorder in a folded protein and its contribution to stability. *J. Am. Chem. Soc.* **121**, 8443–8449 (1999).
71. Bera, M., Ainavarapu, S. R. & Sengupta, K. Significance of 1B and 2B domains in modulating elastic properties of lamin A. *Sci. Rep.* **6**, 27879 (2016).

Acknowledgements

Work in the group of S.J.T. is supported by the Netherlands Organization for Scientific Research (NWO). M.B. and K.F. were supported by a HBIGS PhD fellowship. M.B. was additionally supported by a Boehringer Ingelheim Fonds (BIF) PhD fellowship. J.S. was supported by a fellowship from the Studienstiftung. F.W. received funding from the European Union's Horizon 2020 Research and Innovation Programme under the Marie Skłodowska-Curie grant agreement No 745798. S.J.T. acknowledges a research grant of the European Union (ERC - SyG - 101072047 - CoTransComplex). This work was supported by the Helmholtz-Gemeinschaft (DKFZ NCT3.0 Integrative Project in Cancer Research (DysregPT_Bukau 1030000008 G783)), the European Research Council (ERC Advanced grant (743118), and the Klaus Tschira Foundation. J.S., K.F. and M.B. are members of the Heidelberg Biosciences International Graduate School (HBIGS).

Author contributions

Conceptualization: F.W., J.S., K.T., K.F., M.B., F.T., B.B., G.K., S.J.T. Methodology: F.W., J.S., K.T., K.F., M.B., F.T., B.B., G.K., S.J.T. Biotinylated ribosomes: A.K. Experiments: F.W., J.S., K.T. Formal analysis, and data visualization: J.S., F.W., K.T., K.F., M.B., B.B., G.K., S.J.T. Writing: all authors. Supervision: S.J.T., B.B. and G.K.

Competing interests

The authors declare no competing interests.

Additional information

Supplementary information The online version contains supplementary material available at https://doi.org/10.1038/s41467-025-61500-y.

Correspondence and requests for materials should be addressed to Sander J. Tans.

Peer review information *Nature Communications* thanks the anonymous reviewer(s) for their contribution to the peer review of this work. A peer review file is available.

Reprints and permissions information is available at http://www.nature.com/reprints

Publisher's note Springer Nature remains neutral with regard to jurisdictional claims in published maps and institutional affiliations.

Open Access This article is licensed under a Creative Commons Attribution-NonCommercial-NoDerivatives 4.0 International License, which permits any non-commercial use, sharing, distribution and reproduction in any medium or format, as long as you give appropriate credit to the original author(s) and the source, provide a link to the Creative Commons licence, and indicate if you modified the licensed material. You do not have permission under this licence to share adapted material derived from this article or parts of it. The images or other third party material in this article are included in the article's Creative Commons licence, unless indicated otherwise in a credit line to the material. If material is not included in the article's Creative Commons licence and your intended use is not permitted by statutory regulation or exceeds the permitted use, you will need to obtain permission directly from the copyright holder. To view a copy of this licence, visit http://creativecommons.org/licenses/by-nc-nd/4.0/.

© The Author(s) 2025